

Giant anomalous Nernst effect in the magnetic Weyl semimetal $\text{Co}_3\text{Sn}_2\text{S}_2$

Haiyang Yang¹, Wei You¹, Jialu Wang¹, Junwu Huang¹, Chuanying Xi³,

Chao Cao^{1,*}, Mingliang Tian³, Zhu-An Xu², Jianhui Dai^{1,*}, Yuke Li^{1,*}

¹ *Department of Physics and Hangzhou Key Laboratory of Quantum Matters,
Hangzhou Normal University, Hangzhou 311121, China*

² *Department of Physics,
Zhejiang University, Hangzhou 310027, China*

³ *High Magnetic Field Laboratory,
Chinese Academy of Sciences, Hefei 230031, China*

In ferromagnetic solids, even in absence of magnetic field, a transverse voltage can be generated by a longitudinal temperature gradient. This thermoelectric counterpart of the Anomalous Hall effect (AHE) is dubbed the Anomalous Nernst effect (ANE). Expected to scale with spontaneous magnetization, both these effects arise because of the Berry curvature at the Fermi energy. Here, we report the observation of a giant ANE in a newly-discovered magnetic Weyl semimetal $\text{Co}_3\text{Sn}_2\text{S}_2$ crystal. Hall resistivity and Nernst signal both show sharp jumps at a threshold field and exhibit a clear hysteresis loop below the ferromagnetic transition temperature. The ANE signal peaks a maximum value of $\sim 5 \mu\text{V}/\text{K}$ which is comparable to the largest seen in any magnetic material. Moreover, the anomalous transverse thermoelectric conductivity α_{yx} becomes as large as $\sim 10 \text{ A}/\text{K}\cdot\text{m}$ at 70 K, the largest in known semimetals. The observed ANE signal is much larger than what is expected according to the magnetization.

I. INTRODUCTION

The Nernst effect, the transverse electric field generated by a longitudinal thermal gradient in the presence of a magnetic field, has triggered renewed attention in condensed matter physics since the discovery of the pseudogap phase in cuprates[1, 2]. Conductors with a large Nernst coefficient are important for device applications as in cryogenic refrigerations[3], but such devices have not been realized in practice because of their low conversion efficiency. Recent years, the large Nernst effect has been observed in correlated electron systems[4–6], conventional semimetals[7], as well as in metallic ferromagnets[8–10]. Consequently, a number of novel ground states[4] and exotic electronic orders[6, 11, 12] can be identified by measuring the Nernst effect. For some ferromagnetic metals, in particular, the Nernst signal was observed below T_c even in the absence of external magnetic field[8–10]. This phenomenon, known as the anomalous Nernst effect (ANE), is observed to be proportional to the magnetization. The underlying physics is that the spontaneous magnetization in these materials plays a role of the intrinsic magnetic field, geometrically connected to the Berry curvature of the Bloch bands at the Fermi energy[13].

In recent years topological Dirac/Weyl semimetal materials have been theoretically predicted and experimentally discovered. The electronic structures of these materials have the topologically robust[14–18] and symmetry-protected bulk energy bands which linearly intersect at some special points (the Dirac points) or symmetry axis near the Fermi level[19, 20]. The breaking of inversion symmetry or time-reversal symmetry (TRS) can split a Dirac point into a pair of the Weyl points with opposite chiralities. The chiral Weyl points are then the source or

sink of the Berry curvature $\Omega(k)$ [21], meaning that the Berry curvature is singular at these points. So far, dozens of Dirac/Weyl semimetals have been investigated [22–29] and several unique physical phenomena such as the large magneto-resistivity (MR)[29] and ultrahigh mobility[23] have been observed. However, the defining properties of such topological semimetals, including the Fermi arc in surface states and chiral anomaly in charge transports, are not easy to be identified experimentally. So far, a direct evidence of the Fermi arc has been clarified by ARPES measurements in the TaAs-family[30, 31]. While, a possible indirect signature of the chiral anomaly is associated with the negative longitudinal MR as investigated in several relevant materials[26, 32, 33]. But some extrinsic factors such as the current jetting and crystal inhomogeneity[34] are hardly ruled out.

Quite interestingly, there are two kinds of transverse transport properties, the anomalous Hall effect (AHE) and the anomalous Nernst effect (ANE), can help to probe the topological nature of charge carriers in the ferromagnetic Weyl semimetals. This is because both the transverse transport properties are contributed from the intrinsic magnetic field in the occupied bands and thus deemed as strong proofs of the finite Berry curvature originating from the separation of Weyl nodes. Recently, a magnetic Weyl semimetal $\text{Co}_3\text{Sn}_2\text{S}_2$ with a ferromagnetic kagome-lattice has been reported to show an intrinsic anomalous Hall effect[35, 36], but no experiment on the Nernst effect in this material has been reported yet. It should be noticed that unlike the Hall effect where the normal contribution in a metal is always finite, the Nernst effect generally vanishes in ordinary metals due to the, and thus the anomalous contribution may become very prominent. On the other hand, a large AHE is not necessary to cause a large ANE. This is because the AHE

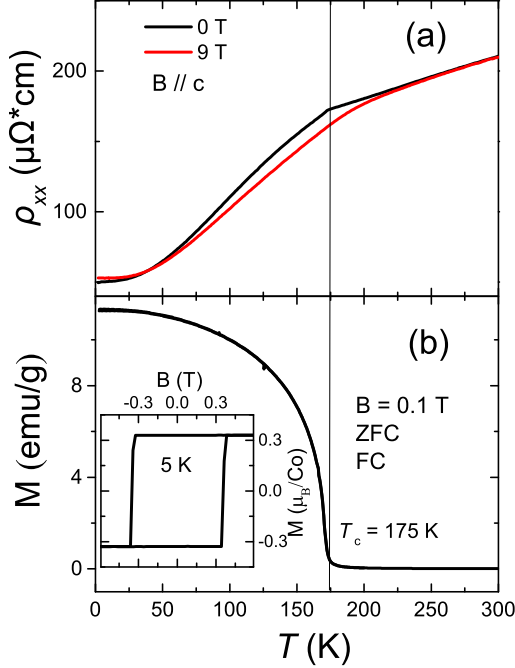


FIG. 1. a Temperature dependence of the longitudinal electric resistivity (ρ_{xx}) of $\text{Co}_3\text{Sn}_2\text{S}_2$ sample under zero field and 9 T. b Temperature dependence of magnetization with the FC modes at $B = 0.1$ T. The inset shows the saturated magnetization vs. fields at 5 K.

is determined by the integration of the Berry curvature from all occupied bands, while the ANE is governed by the Berry curvature at the Fermi level[13, 37]. Thus, studying the ANE is highly useful to confirm the contribution of the Berry curvature and in turn verify the intrinsic Weyl state in a Weyl semimetal.

In this paper, we systematically study the ANE in the magnetic Weyl semimetal $\text{Co}_3\text{Sn}_2\text{S}_2$. We find that the ANE signal reaches a maximum value of $\sim 5 \mu\text{V/K}$ at 70 K, yielding a giant transverse thermoelectrical conductivity of $\sim 10 \text{ A/K.m}$, much larger than those of known ferromagnetic metals. This result shows that $\text{Co}_3\text{Sn}_2\text{S}_2$ is an idea material candidate for future device application in cryogenic refrigerations. Our study also provide insights in understanding the intrinsic Weyl state and the correlation between AHE and ANE.

II. RESULTS AND DISCUSSION

$\text{Co}_3\text{Sn}_2\text{S}_2$ crystallizes in a rhombohedral structure with the space group of R-3m. Co atoms form a kagome lattice with corner-sharing triangles of Co atoms in the CoSn-layer, and the kagome lattices in different layers are stacked along the c-axis with a corner-sharing octahedra. The sample shows a magnetic moment of $\sim 0.33\mu_B/\text{Co}$

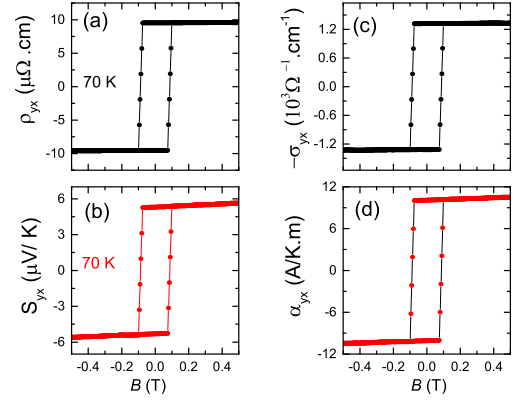


FIG. 2. Field dependence of transport coefficients at 70 K as $B \parallel c$ -axis $\perp I$. (a) Hall resistivity ρ_{yx} vs. magnetic fields. (b) The Nernst signal S_{yx} . (c) The Hall conductivity σ_{yx} , extracted from ρ_{xx} and ρ_{yx} . (d) Transverse thermoelectric conductivity α_{yx} , extracted from ρ_{xx} , ρ_{yx} , S_{xx} and S_{yx} . The hysteretic behavior is clearly observed at 70 K.

along the c-axis with a Neel temperature of about 175 K in figure 1b. The FC and ZFC curves overlap each other very well at 0.1 T, implying that the magnetic domains have been arranged along c-axis by the small external fields. The clear hysteresis loop with the saturated magnetization M_s of $0.33 \mu_B/\text{Co}$ at 5 K is observed in the inset of figure 1b, consistent with the theoretical prediction[35, 36]. Temperature dependence of longitudinal resistivity ρ_{xx} and thermopower S_{xx} of $\text{Co}_3\text{Sn}_2\text{S}_2$ single crystal are shown in figure 1a. Overall the resistivity shows a metallic behavior in the whole temperature regime but exhibits an unexpected kink associated with a ferromagnetic transition(FM) at about $T_c = 175$ K, similar to the previous report[38]. As a magnetic field up to 9 T is applied, the resistivity does not change too much at high temperature but starts to decrease below 200 K. The kink in $\rho_{xx}(T)$ near T_c broadens and becomes very smooth under 9 T, as seen in the literatures[35, 36].

Figure 2a and 2c display the Hall resistivity and conductivity vs. the applied magnetic fields $B \parallel c \perp I$ at a representative temperature of 70 K. The $\rho_{yx}(B)$ significantly exhibits a steep rectangular hysteretic jump at low fields, and then becomes almost flat at a higher field. Its magnitude is comparable to what was reported previously[35, 36] and is reversible with a field of 0.15 T at 70 K. The largest coercive field is about 0.7 T at 5 K (See figure S3 in SI). The Nernst signal S_{yx} (figure 2b) shows a similar jump of about $10 \mu\text{V/K}$, which is over one order of magnitude larger than those of typical materials for the ANE such as Mn_3Sn [39], pure metal Fe[40] $\text{CuCr}_2\text{Se}_{4-x}\text{Br}_x$ [9] and single crystal Fe_3O_4 [10]. The large S_{yx} is also verified by the large Nernst angle $\theta_N = |S_{yx}/S_{xx}|$ of 16% (Figure 3b). Note that both Hall resistivity and Nernst signal show nearly the same magnetic field dependence as the magnetization curve (See figure S2 in SI), implying that the contribution of

the anomalous Hall and Nernst effects dominates and the normal contribution (proportional to B) is negligibly small at low fields.

Field dependence of the Hall conductivity $-\sigma_{yx}$ and the transverse thermoelectric conductivity α_{yx} at 70 K is shown in figure 2c and 2d. The σ_{yx} and α_{yx} can be written as the formulas $\sigma_{yx} = -\rho_{yx}/(\rho_{yx}^2 + \rho^2)$ and $\alpha_{yx} = (\rho_{xx}S_{yx} - \rho_{yx}S_{xx})/\rho_{xx}^2$ [40]. The obtained $|\sigma_{yx}|$ at the saturated field 0.5 T reaches ~ 1320 (Ωcm) $^{-1}$, which is very close to the calculated result (1310 (Ωcm) $^{-1}$) from the integral of Berry curvature along k_z in the system [35, 36]. Similar to the large σ_{yx} , the α_{yx} is found to be very large, reaching approximately 11 A/K.m at 70 K. This value is one or two orders magnitude of larger than the other typical ferromagnets or Mn_3Sn with $\alpha_{yx} \sim 0.01 - 1$ A/K.m, as shown in Figure 4b.

Temperature dependence of the AHR, ρ_{yx}^A , (extrapolating the high-field part of ρ_{yx} back to zero field) and AHC, σ_{xy}^A , are illustrated in figure 3a. The ρ_{yx}^A shows a strong temperature-dependence below T_c , and peaks a maximum value of $21 \mu\Omega\text{cm}$ around 140 K. While the σ_{xy}^A is almost temperature-independence below 100 K. Such feature is also observed in pure materials such as Fe, Co, Ni and Gd, where the mechanism of the AHE has been suggested to be the intrinsic Berry-phase mechanism[8]. We plot the σ_{xy}^A as a function of σ_{xx} in the main plane of figure 3b. It describes that σ_{xy}^A is weakly dependent of σ_{xx} at low temperature regime (< 100 K), similar to the case in Fe, Ni pure metals[8] (See SI). A large anomalous Hall angle $|\sigma_{xy}^A/\sigma|$ reaches a maximum value about 15% at 150 K and gradually decreases to 6.3% at 5 K, as shown in the inset of figure 3b. The large Hall angle in $\text{Co}_3\text{Sn}_2\text{S}_2$ is close to the value of 16% in GdPtBi , a typical field-induced Weyl-semimetal[41], but is much larger than that of the noncolinear antiferromagnetic Mn_3Sn (3.2%)[42] and Mn_3Ge (5%)[39].

The ANE signal S_{yx}^A as a function of temperature is displayed in figure 3c. The S_{yx}^A strongly depends on temperature, rapidly increases below T_c and then peaks at around 70 K, a half of the peak temperature of ρ_{yx}^A in figure 3a. Similar to the large Hall angle, the large S_{yx}^A can be verified by the Nernst angle $\theta_N = |S_{yx}/S_{xx}|$ in the inset of figure 3c. The value reaches 17% at 70 K, which is comparable with the previous findings in the Co_2MnGa system[43], a FM semimetal. Correspondingly, temperature dependence of the α_{yx}^A is mapped in the inset of figure 3d, and the α_{yx}^A rapidly increases below 200 K, showing a maximum value of ~ 11 A/K.m at 50 K, followed by a monotonous decrease to low temperatures. Such large α_{yx}^A is one or two orders magnitude larger than the other ferromagnets with a small $\alpha_{yx} \sim 0.01-1$ A/K.m (See figure S4 in SI). Note that the α_{yx}^A is roughly obey the linear T-dependence at low temperatures, but closely follow the relation $\propto T \log(T)$ at a temperature regime from 70 K to 175 K, as shown in figure 3d. Similar behavior has been reported in Co_2MnGa system[43].

The significant difference between the giant ANE in

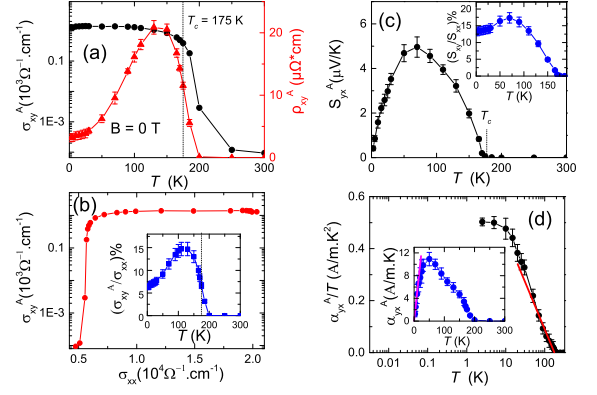


FIG. 3. (a) Temperature dependence of the anomalous Hall conductivity σ_{xy}^A and Hall resistivity ρ_{yx}^A at zero magnetic field. (b) $(\sigma_{xy})^A$ as a function of σ_{xx} in the main plane. The inset shows temperature dependence of the Hall angle ($|\sigma_{xy}^A/\sigma|$) at zero magnetic field. (c) Temperature dependence of the anomalous Nernst signal S_{yx}^A . The inset shows the Nernst angle $|\theta_N = S_{yx}/S_{xx}|$ as a function of temperature. (d) Temperature dependence of the α_{yx}^A/T . The inset shows the transverse thermoelectric conductivity α_{yx} vs. temperature.

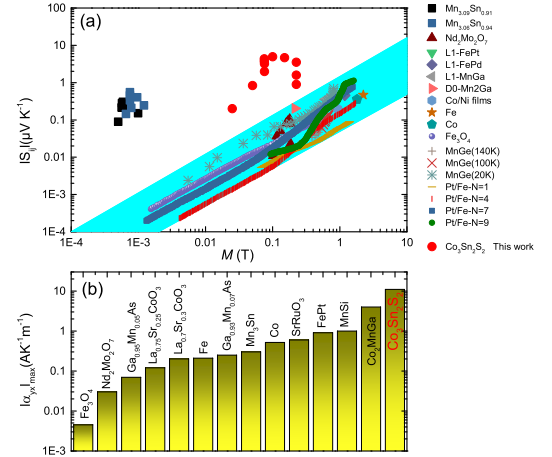


FIG. 4. (a) Magnetization dependence of the spontaneous Nernst effect for FM metals, Mn_3Sn and $\text{Co}_3\text{Sn}_2\text{S}_2$. (b) The transverse thermoelectric conductivity $|\alpha_{yx}|$ vs. the various ferromagnets, Mn_3Sn and $\text{Co}_3\text{Sn}_2\text{S}_2$. All those ANE results are obtained for various ferromagnets below their Curie temperatures(Methods).

$\text{Co}_3\text{Sn}_2\text{S}_2$, Mn_3Sn and in ferromagnets is demonstrated in figure 4a. We plot the ANE as functions of the magnetization with a logarithmic scale for various ferromagnetic metals, Mn_3Sn and $\text{Co}_3\text{Sn}_2\text{S}_2$ (See Methods). The ANE in ferromagnets is known to be roughly proportional to the magnetization M , $|S_{yx}| = |Q_s|\mu_0 M$, where $|Q_s|$ is the anomalous Nernst coefficient. It can be seen that almost all of ferromagnetic metals follow this re-

lation and their ANE signal becomes more larger with increasing magnetization. The shaded region covers all of the data points for ferromagnets. An exception for the antiferromagnetic Mn_3Sn observed strongly violates this scaling, which is ascribed to the enhanced Berry curvature at the Fermi energy[42]. Similarly, the $\text{Co}_3\text{Sn}_2\text{S}_2$ does not follow this relation. The S_{yx} is concretely far away from this trend and more than one and two order magnitude larger than what would be expected based on the scaling relation. In addition, the intrinsic transverse thermoelectric conductivity $|\alpha_{yx}|$ is close to 11 A/K.m for $\text{Co}_3\text{Sn}_2\text{S}_2$, the largest value compared to the other ferromagnets and semimetals as shown in figure 4b. The observed large $|\alpha_{yx}|$ in the Weyl magnets are potentially useful to realize the thermoelectric devices for cryogenic refrigeration.

The mechanism of the significantly large intrinsic ANE in $\text{Co}_3\text{Sn}_2\text{S}_2$ should be distinct from the conventional one for ferromagnets. In the formwork of the Boltzmann approach, the anomalous Hall conductivity σ_{yx}^A and the anomalous transverse thermoelectric conductivity α_{yx}^A can be written as the formulas[37]: $\sigma_{yx}^A = -\frac{e^2}{\hbar} \int \frac{dk}{2\pi^3} \Omega_{n,z}(k) f_{nk}$, and $\alpha_{yx}^A = -\frac{e}{T\hbar} \int \frac{dk}{2\pi^3} \Omega_{n,z}(k) (\varepsilon_{n,k} - \mu) f_{n,k} + k_B T \ln[1 + e^{-\beta(\varepsilon_{n,k} - \mu)}]$. Here, $\Omega_{n,k}$ is the Berry curvature along the z direction, and $f_{nk} = f(E_{nk})$ is the Fermi distribution function with the band index n and the wave vector k . $\varepsilon_{n,k}$ and β donate the band energy and $1/k_B T$. From the equations, the α_{yx}^A is governed by the Berry curvature around the Fermi energy, while the σ_{yx}^A is given by the summation of the Berry curvature for all the occupied bands. According to these equations, the α_{yx}^A at low temperatures can be reduced to the Mott relations $\alpha_{yx}^A = \frac{\pi^2 k_B^2 T}{4e} \frac{\partial \sigma_{yx}^A}{\partial \varepsilon}$. Our result in $\alpha_{yx}^A(T)$ showing a roughly linear temperature-dependence at low temperatures is consistent with the Mott rule.

III. CONCLUSION

In summary, we report an observation of the giant ANE and the large intrinsic transverse thermoelectric conductivity in the magnetic Weyl semimetal $\text{Co}_3\text{Sn}_2\text{S}_2$. The Nernst signal S_{yx} reaches $\sim 5 \mu\text{V/K}$ at 70 K, much larger than those of known ferromagnetic metals. Furthermore, the $\alpha_{xy}^A \sim 10\text{A/K.m}$ in the sample is over one or two order magnitude larger than those of other ferromagnets where $\alpha_{xy}^A = 0.01 - 1\text{A/K.m}$. Our experimental results indicate that the giant ANE in $\text{Co}_3\text{Sn}_2\text{S}_2$ can

be ascribed to the enhanced contribution from the Berry curvature very close to Fermi levels. The enhanced α_{xy} in Weyl magnets paves a path to realize potentially thermopile devices for the thermoelectric power generation. Our experimental results also highlight the complementary roles of ANE and AHE in revealing the intrinsic Weyl state in the magnetic Weyl semimetals.

IV. METHOD

Large single crystals of $\text{Co}_3\text{Sn}_2\text{S}_2$ with the millimeter size were grown through the Bridgman technique, as reported in the previous reports[38].

The single crystal X-ray diffraction were obtained using a D/Max-rA diffractometer with $\text{CuK}\alpha$ radiation and a graphite monochromator at the room temperature, which determines the crystal grown orientation. The composition of the crystals were obtained by energy dispersive X-ray (EDX) spectroscopy. The sample is polished and then cut into a bar-shape with a size of $3.5 \times 2 \times 0.2\text{mm}^3$. The magnetization measurements were done using a commercial SQUID magnetometer. The (magneto)resistivity and Hall coefficient measurements were performed using the standard four-terminal method in a commercial Quantum Design PPMS-9 system. The thermal power measurement were performed with a one-heater-two-thermometers technique in PPMS with a high-vacuum environment. Two Chromel-constantan (type E) thermocouples were employed to measure the temperature difference generated by a small heater chip.

In figure4a, the Nernst signal S_{yx} for various ferromagnets below the Curie temperatures is abstracted the ANE results, as reported in those literatures. For example Fe(300 K)[44]; Co(300K)[44]; Fe_3O_4 (300K)[10]; MnGe(140K)[45], MnGe(100K)[45] and MnGe(20K)[45]; $\text{Nd}_2\text{Mo}_2\text{O}_7$ [46]; Co/Ni film(300K)[47]; Pt/Fe multilayer(300K)[48]; MnGa(300K)[47]; Mn_2Ga (300K)[47]; FePt(300K)[47]; and FePd(300K)[47]; Mn_3Sn [42]

In figure 4b, the maximum $|\alpha_{xy}^A|$ values are taken from each magnetic material, Mn_3Sn and Co_2MnGa . $|\alpha_{xy}^A| \sim 1\text{A/Km}$ for MnSi[49], $|\alpha_{xy}^A| \sim 0.6\text{A/Km}$ for SrRuO₃[8], $|\alpha_{xy}^A| \sim 0.3\text{A/Km}$ for Mn_3Sn [42], $|\alpha_{xy}^A| \sim 0.2$ and 0.12A/Km for $\text{La}_{1-x}\text{Sr}_x\text{CoO}_3$ ($x=0.3$ and 0.25)[8], $|\alpha_{xy}^A| \sim 0.03\text{A/Km}$ for $\text{Nd}_2\text{Mo}_2\text{O}_7$ [46], $|\alpha_{xy}^A| \sim 0.25$ and 0.07A/Km for $\text{Ga}_{1-x}\text{Mn}_x\text{Si}$ [50], $|\alpha_{xy}^A| \sim 0.0045\text{A/Km}$ for Fe_3O_4 [10], and $|\alpha_{xy}^A| \sim 0.9, 0.52$ and 0.21A/Km for FePt, Co and Fe[51], $|\alpha_{xy}^A| \sim 4\text{A/Km}$ for Co_2MnGa [43], and $|\alpha_{xy}^A| \sim 11\text{A/Km}$ for $\text{Co}_3\text{Sn}_2\text{S}_2$.

[1] ZA Xu, NP Ong, Yayu Wang, T Kakeshita, and S Uchida. Vortex-like excitations and the onset of superconducting phase fluctuation in underdoped $\text{La}_{2-x}\text{Sr}_x\text{CuO}_4$. *Nature*, 406(6795):486, 2000.

[2] Yayu Wang, Lu Li, and N. P. Ong. Nernst effect in high- T_c superconductors. *Phys. Rev. B*, 73:024510, Jan 2006.

[3] Franz Freibert, Timothy W Darling, Albert Migliori, and Stuart A Trugman. Thermomagnetic effects and

- measurements. In *Semiconductors and Semimetals*, volume 70, pages 207–244. Elsevier, 2001.
- [4] Kamran Behnia. The nernst effect and the boundaries of the fermi liquid picture. *Journal of Physics: Condensed Matter*, 21(11):113101, 2009.
- [5] R. Bel, K Behnia, Y Nakajima, K Izawa, Y Matsuda, H Shishido, R Settai, and Y Onuki. Giant nernst effect in CeCoIn₅. *Physical Review Letters*, 92(21):217002, 2004.
- [6] Romain Bel, Hao Jin, Kamran Behnia, Jacques Flouquet, and Pascal Lejay. Thermoelectricity of URu₂Si₂: Giant nernst effect in the hidden-order state. *Phys. Rev. B*, 70:220501, Dec 2004.
- [7] Kamran Behnia, Marie-Aude Méasson, and Yakov Kopelevich. Nernst effect in semimetals: The effective mass and the figure of merit. *Physical Review Letters*, 98(7):076603, 2007.
- [8] T. Miyasato, N. Abe, T. Fujii, A. Asamitsu, S. Onoda, Y. Onose, N. Nagaosa, and Y. Tokura. Crossover behavior of the anomalous hall effect and anomalous nernst effect in itinerant ferromagnets. *Phys. Rev. Lett.*, 99:086602, Aug 2007.
- [9] Wei-Li Lee, S. Watauchi, V. L. Miller, R. J. Cava, and N. P. Ong. Anomalous hall heat current and nernst effect in the CuCr₂Se_{4-x}Br_x ferromagnet. *Phys. Rev. Lett.*, 93:226601, Nov 2004.
- [10] R. Ramos, M. H. Aguirre, A. Anadón, J. Blasco, I. Lucas, K. Uchida, P. A. Algarabel, L. Morellón, E. Saitoh, and M. R. Ibarra. Anomalous nernst effect of Fe₃O₄ single crystal. *Phys. Rev. B*, 90:054422, Aug 2014.
- [11] A. Pourret, K. Behnia, D. Kikuchi, Y. Aoki, H. Sugawara, and H. Sato. Drastic change in transport of entropy with quadrupolar ordering in PrFe₄P₁₂. *Phys. Rev. Lett.*, 96:176402, May 2006.
- [12] Francis Lalibert David LeBoeuf Nicolas Doiron-Leyraud J. Chang J. Q. Yan J.-G. Cheng J.-S. Zhou J. B. Goodenough S. Pyon T. Takayama H. Takagi Y. Tanaka Louis Taillefer Olivier Cyr-Choinire, R. Daou. Enhancement of the nernst effect by stripe order in a high-*t_c* superconductor. *Nature*, 458:743, 2009.
- [13] Di Xiao, Yugui Yao, Zhong Fang, and Qian Niu. Berry-phase effect in anomalous thermoelectric transport. *Physical Review Letters*, 97(2):026603, 2006.
- [14] N. P. Armitage, E. J. Mele, and Ashvin Vishwanath. Weyl and dirac semimetals in three-dimensional solids. *Rev. Mod. Phys.*, 90:015001, Jan 2018.
- [15] Xiangang Wan, Ari M. Turner, Ashvin Vishwanath, and Sergey Y. Savrasov. Topological semimetal and fermi-arc surface states in the electronic structure of pyrochlore iridates. *Phys. Rev. B*, 83:205101, May 2011.
- [16] S. M. Young, S. Zaheer, J. C. Y. Teo, C. L. Kane, E. J. Mele, and A. M. Rappe. Dirac semimetal in three dimensions. *Phys. Rev. Lett.*, 108:140405, Apr 2012.
- [17] Kai-Yu Yang, Yuan-Ming Lu, and Ying Ran. Quantum hall effects in a weyl semimetal: Possible application in pyrochlore iridates. *Phys. Rev. B*, 84:075129, Aug 2011.
- [18] Chen Fang, Matthew J. Gilbert, Xi Dai, and B. Andrei Bernevig. Multi-weyl topological semimetals stabilized by point group symmetry. *Phys. Rev. Lett.*, 108:266802, Jun 2012.
- [19] A. A. Burkov, M. D. Hook, and Leon Balents. Topological nodal semimetals. *Phys. Rev. B*, 84:235126, Dec 2011.
- [20] Gang Xu, Hongming Weng, Zhijun Wang, Xi Dai, and Zhong Fang. Chern semimetal and the quantized anomalous hall effect in HgCr₂Se₄. *Phys. Rev. Lett.*, 107:186806, Oct 2011.
- [21] Shuichi Murakami and Shun-ichi Kuga. Universal phase diagrams for the quantum spin hall systems. *Phys. Rev. B*, 78:165313, Oct 2008.
- [22] Zhijun Wang, Hongming Weng, Quansheng Wu, Xi Dai, and Zhong Fang. Three-dimensional dirac semimetal and quantum transport in cd₃as₂. *Phys. Rev. B*, 88:125427, Sep 2013.
- [23] Tian Liang, Quinn Gibson, Mazhar N Ali, Minhao Liu, RJ Cava, and NP Ong. Ultrahigh mobility and giant magnetoresistance in the dirac semimetal Cd₃As₂. *Nature materials*, 14(3):280–284, 2015.
- [24] Zhijun Wang, Yan Sun, Xing-Qiu Chen, Cesare Franchini, Gang Xu, Hongming Weng, Xi Dai, and Zhong Fang. Dirac semimetal and topological phase transitions in A₃Bi (A = Na, K, Rb). *Physical Review B*, 85(19):195320, 2012.
- [25] Hongming Weng, Chen Fang, Zhong Fang, B Andrei Bernevig, and Xi Dai. Weyl semimetal phase in noncentrosymmetric transition-metal monophosphides. *Physical Review X*, 5(1):011029, 2015.
- [26] Frank Arnold, Chandra Shekhar, Shu-Chun Wu, Yan Sun, Ricardo Donizeth Dos Reis, Nitesh Kumar, Marcel Naumann, Mukkattu O Ajeesh, Marcus Schmidt, Adolfo G Grushin, et al. Negative magnetoresistance without well-defined chirality in the weyl semimetal TaP. *Nature communications*, 7, 2016.
- [27] Chandra Shekhar, Ajaya K Nayak, Yan Sun, Marcus Schmidt, Michael Nicklas, Inge Leermakers, Uli Zeitler, Yurii Skourski, Jochen Wosnitza, Zhongkai Liu, et al. Extremely large magnetoresistance and ultrahigh mobility in the topological weyl semimetal candidate NbP. *Nature Physics*, 11(8):645–649, 2015.
- [28] Nirmal Jeevi Ghimire, Yongkang Luo, Madhab Neupane, DJ Williams, ED Bauer, and F Ronning. Magnetotransport of single crystalline NbAs. *Journal of Physics: Condensed Matter*, 27(15):152201, 2015.
- [29] Cheng-Long Zhang, Zhujun Yuan, Qing-Dong Jiang, Bingbing Tong, Chi Zhang, XC Xie, and Shuang Jia. Electron scattering in tantalum monoarsenide. *Physical Review B*, 95(8):085202, 2017.
- [30] Shin-Ming Huang, Su-Yang Xu, Ilya Belopolski, Chi-Cheng Lee, Guoqing Chang, BaoKai Wang, Nasser Alidoust, Guang Bian, Madhab Neupane, Chenglong Zhang, et al. A weyl fermion semimetal with surface fermi arcs in the transition metal monpnictide TaAs class. *Nature communications*, 6:7373, 2015.
- [31] Su-Yang Xu, Ilya Belopolski, Nasser Alidoust, Madhab Neupane, Guang Bian, Chenglong Zhang, Raman Sankar, Guoqing Chang, Zhujun Yuan, Chi-Cheng Lee, et al. Discovery of a weyl fermion semimetal and topological fermi arcs. *Science*, 349(6248):613–617, 2015.
- [32] Jun Xiong, Satya K Kushwaha, Tian Liang, Jason W Krizan, Max Hirschberger, Wudi Wang, RJ Cava, and NP Ong. Evidence for the chiral anomaly in the dirac semimetal Na₃Bi. *Science*, 350(6259):413–416, 2015.
- [33] Yuke Li, Lin Li, Jialu Wang, Tingting Wang, Xiaofeng Xu, Chuanying Xi, Chao Cao, and Jianhui Dai. Resistivity plateau and negative magnetoresistance in the topological semimetal TaSb₂. *Physical Review B*, 94(12):121115, 2016.
- [34] RD Dos Reis, MO Ajeesh, N Kumar, F Arnold, C Shekhar, M Naumann, M Schmidt, M Nicklas, and

- E Hassinger. On the search for the chiral anomaly in weyl semimetals: The negative longitudinal magnetoresistance. *New Journal of Physics*, 18(8):085006, 2016.
- [35] Enke Liu, Yan Sun, Nitesh Kumar, Lukas Muechler, Aili Sun, Lin Jiao, Shuo-Ying Yang, Defa Liu, Aiji Liang, Qianan Xu, et al. Giant anomalous hall effect in a ferromagnetic kagome-lattice semimetal. *Nature Physics*, page 1, 2018.
- [36] Qi Wang, Yuanfeng Xu, Rui Lou, Zhonghao Liu, Man Li, Yaobo Huang, Dawei Shen, Hongming Weng, Shancai Wang, and Hechang Lei. Large intrinsic anomalous hall effect in half-metallic ferromagnet $Co_3Sn_2S_2$ with magnetic weyl fermions. *Nature Communications*, 9(1):3681, 2018.
- [37] Di Xiao, Ming-Che Chang, and Qian Niu. Berry phase effects on electronic properties. *Reviews of Modern Physics*, 82(3):1959, 2010.
- [38] Mohamed A. Kassem, Yoshikazu Tabata, Takeshi Waki, and Hiroyuki Nakamura. Low-field anomalous magnetic phase in the kagome-lattice shandite $Co_3Sn_2S_2$. *Phys. Rev. B*, 96:014429, Jul 2017.
- [39] Ajaya K Nayak, Julia Erika Fischer, Yan Sun, Binghai Yan, Julie Karel, Alexander C Komarek, Chandra Shekhar, Nitesh Kumar, Walter Schnelle, Jürgen Kübler, et al. Large anomalous hall effect driven by a nonvanishing berry curvature in the noncolinear antiferromagnet Mn_3Ge . *Science advances*, 2(4):e1501870, 2016.
- [40] Xiaokang Li, Liangcai Xu, Linchao Ding, Jinhua Wang, Mingsong Shen, Xiufang Lu, Zengwei Zhu, and Kamran Behnia. Anomalous nernst and righi-leduc effects in Mn_3Sn : Berry curvature and entropy flow. *Phys. Rev. Lett.*, 119:056601, Aug 2017.
- [41] T. Suzuki, R. Chisnell, A. Devarakonda, Y. T. Liu, W. Feng, and D. Xiao. Large anomalous hall effect in a half-heusler antiferromagnet. *Nature Physics*, 12:1119, 2016.
- [42] Tomita Takahiro Koretsune Takashi Suzuki Michi-To Nishio-Hamane-Daisuke Arita Ryotaro Otani Yoshichika Nakatsuji Satoru Ikhlas, Muhammad. Large anomalous nernst effect at room temperature in a chiral antiferromagnet. *Nature Physics*, 13:1085, 2017.
- [43] Akito Sakai, Yo Pierre Mizuta, Agustinus Agung Nugroho, Rombang Sihombing, Takashi Koretsune, Michi-To Suzuki, Nayuta Takemori, Rieko Ishii, Daisuke Nishio-Hamane, Ryotaro Arita, et al. Giant anomalous nernst effect and quantum-critical scaling in a ferromagnetic semimetal. *Nature Physics*, page 1, 2018.
- [44] John P Perdew, Kieron Burke, and Matthias Ernzerhof. Generalized gradient approximation made simple. *Physical review letters*, 77(18):3865, 1996.
- [45] David Vanderbilt. Soft self-consistent pseudopotentials in a generalized eigenvalue formalism. *Physical Review B*, 41(11):7892, 1990.
- [46] N Hanasaki, K Sano, Y Onose, T Ohtsuka, S Iguchi, I Kézsmárki, S Miyasaka, S Onoda, N Nagaosa, and Y Tokura. Anomalous nernst effects in pyrochlore molybdates with spin chirality. *Physical review letters*, 100(10):106601, 2008.
- [47] K Hasegawa, M Mizuguchi, Y Sakuraba, T Kamada, T Kojima, T Kubota, S Mizukami, T Miyazaki, and K Takanashi. Material dependence of anomalous nernst effect in perpendicularly magnetized ordered-alloy thin films. *Applied Physics Letters*, 106(25):252405, 2015.
- [48] Arash A Mostofi, Jonathan R Yates, Young-Su Lee, Ivo Souza, David Vanderbilt, and Nicola Marzari. wannier90: A tool for obtaining maximally-localised wannier functions. *Computer physics communications*, 178(9):685–699, 2008.
- [49] Yuji Hirokane, Yasuhide Tomioka, Yoshinori Imai, Atsutaka Maeda, and Yoshinori Onose. Longitudinal and transverse thermoelectric transport in mnsi. *Physical Review B*, 93(1):014436, 2016.
- [50] Yong Pu, Daichi Chiba, Fumihiko Matsukura, Hideo Ohno, and Jing Shi. Mott relation for anomalous hall and nernst effects in $Ga_{1-x}Mn_xAs$ ferromagnetic semiconductors. *Physical review letters*, 101(11):117208, 2008.
- [51] Jürgen Weischenberg, Frank Freimuth, Stefan Blügel, and Yuriy Mokrousov. Scattering-independent anomalous nernst effect in ferromagnets. *Physical Review B*, 87(6):060406, 2013.

ACKNOWLEDGEMENTS

We thank K. Behnia for inspiring discussions and suggestions. We also thank H. Wang, and J. Yang for some technical support. This research was supported in part by the NSF of China (under Grants No. 11474082) and the National Key Projects for Research and Development of China (Contract No. 2016YFA0300402). Yu-Ke Li was supported by an open program from Wuhan National High Magnetic Field Center (2016KF03).

AUTHOR CONTRIBUTIONS

Y. Li designed the research. H. Yang synthesized the samples and performed the electronic and thermal transport measurements. W. You performed the XRD measurements and analyzed the structure parameters. C. Cao performed the first-principle calculation. C. Xi, and J. Wang assisted the measurements. C. Cao, M. L. Tian, Z. A. Xu, J. Dai, and Y. Li, discussed the data, interpreted the results. J. Dai and Y. Li wrote the paper.

ADDITIONAL INFORMATION

Competing financial interests: The authors declare no competing financial interests. Correspondence and requests for materials should be addressed to Yuke Li (email: yklee@hznu.edu.cn).